Hydrogen in Nanostructured, Carbon-Related, and Metallic Materials

Andreas Züttel and Shin-ichi Orimo

Abstract

Recent developments in hydrogen interaction with carbonaceous materials are reviewed in this article. The interaction is based on van der Waals attractive forces (physisorption), or the overlap of the highest occupied molecular orbitals of carbon with the hydrogen electron, overcoming the activation-energy barrier for hydrogen dissociation (chemisorption). While the physisorption of hydrogen limits the hydrogen-to-carbon ratio to less than one hydrogen atom per two carbon atoms (i.e., 4.2 mass%), in chemisorption, a ratio of two hydrogen atoms per one carbon atom is realized (e.g., in polyethylene). However, the materials with large hydrogen-to-carbon ratios only liberate the hydrogen at elevated temperature. No evidence, apart from theoretical calculations, was found for a new hydrogen-adsorption phenomenon on carbon nanotubes (CNTs), as compared with high-surface-area graphite. The curvature of CNTs and fullerenes increases the reactivity of these materials with hydrogen and leads more easily to the formation of hydrocarbons, as compared with graphite. Nanocrystalline or amorphous carbon exhibits an intermediate state for hydrogen between physisorption and chemisorption and absorbs up to one hydrogen atom per carbon atom. Nanostructured carbonaceous and metallic materials offer a large potential for hydrogen storage and must therefore be investigated in more detail.

Keywords: *adsorption, carbon nanotubes, chemical reactivity, hydrogen storage, nanofibers.*

Preparation of Carbon Nanostructures

Synthesis of Nanotubes and Nanofibers

In 1991, Iijima[1] described for the first time the new form of carbon called carbon nanotubes (CNTs). CNTs are rolled graphite sheets with an inner diameter ranging from 0.7 nm up to several nanometers and a length of 10–100 μm. They are usually closed on both ends by a hemisphere, that is, half of a fullerene. Nanotubes formed from a single graphite layer are called single-walled nanotubes (SWNTs). Nanotubes consisting of multiple concentric graphite layers are called multiwalled nanotubes (MWNTs). The interlayer distance in a MWNT is close to the interlayer distance in graphite, which is equal to half of the unit-cell parameter c ($0.5c = 0.3355$ nm). The diameters of SWNTs vary from 0.671 nm to 3 nm, whereas MWNTs show typical diameters of 30–50 nm. The helicity of the nanotubes is usually described by the Hamada vector,[2] which indicates how the graphene sheet is rolled up along a lattice vector with components (n,m). The values of the integers n and m identify the general geometry of a SWNT. Nanotubes with $n = m$ are called "armchair"; nanotubes with either $n = 0$ or $m = 0$ are called "zigzag"; all others have chiral symmetry.[3] SWNTs tend to agglomerate and form bundles of several tens of nanotubes. The nanotubes in the bundles are in two dimensions and close-packed, and the intertube distance is 0.334 nm.[4]

Carbon fibers are similar to carbon nanotubes except for their inner structure. Carbon fibers consist of graphite platelets stacked together, with an interlayer spacing of 0.3355 nm, in various orientations with respect to the fiber axis, giving rise to assorted conformations. Three types of carbon fibers can be distinguished. In the platelet-like carbon fiber, the area vector of the graphene sheets is parallel to the axis of the fiber. These fibers can be easily distinguished from nanotubes, as they do not exhibit a concentric hole (i.e., are not tube-like), and the shadow lines in transmission electron microscopy (TEM) images are perpendicular to the fiber axis.

The ribbon-like fibers consist of continuous graphene layers along the axis of the fibers. This type of fiber exhibits a very similar pattern to the SWNTs in TEM images.

The herringbone fibers are an intermediate type of the platelet- and ribbon-like fibers and consist of graphite platelets with an area vector oriented 45° to the axis of the fiber.

Several methods have been developed to synthesize carbon nanostructures. All of them—laser vaporization, electric-arc discharge, and chemical vapor deposition—work at elevated temperatures (>800 K), and metal particles (e.g., Fe, Co, or Ni) are involved in the reaction. The details of the synthesis of carbon nanostructures were reviewed by Ding et al.[5] The large variety of carbon nanostructures with presumably different physical and chemical properties turned out to be the major difficulty in the interpretation of the experimental results. Many of the structures appear simultaneously in the synthesis. Therefore, most of the samples are not homogeneous. In contrast to the buckminsterfullerenes, which can be purified by chemical extraction, nanotubes, with their large aspect ratio (often >1000), are very difficult to purify. Furthermore, most experiments were performed with small sample quantities of a few milligrams and could not be repeated with the same type of sample. This fact makes the inconsistent results understandable. It is a challenge to develop methods for the synthesis of homogeneous, well-defined nanotubes.

Preparation of Highly Defective Carbon

The capillary effects that originate from ideal tube-like structures are assumed to provide dominant hydrogen storage/trapping sites in CNTs. Pretreatments prior to hydrogenation, however, seem to increase the number of defects, such as dangling carbon bonds, even in the side walls of the CNTs.[6] Therefore, hydrogen-storage properties that are improved by the defective structures should be taken into account in nanostructured carbon-

related materials. One of the effective methods for preparing highly defective structures in carbon-related materials is mechanical milling.[7–17] This primitive but reliable method may provide a new category of carbon-related materials for hydrogen storage, in which hydrogen is weakly chemisorbed (bonded) by the defective structures.[18–20]

Hydrogen Storage Using Carbon Nanostructures

Interaction with Molecular Hydrogen

Much of the work on reversible hydrogen sorption by carbon nanostructures was stimulated by the findings published in an article by Dillon et al.[21] This paper described the results of a brief hydrogen-desorption experiment. The authors estimated the hydrogen-storage capacity of CNTs at that time to be 5–10 mass%. The investigation was carried out on a carbon sample containing an estimated amount (by TEM micrographs) of 0.1–0.2 mass% SWNTs. The amount of hydrogen desorbed in the high-temperature chemisorption peak, which is roughly 5–10 times smaller than the low-temperature physisorption peak, was 0.01 mass%. The authors concluded that the gravimetric storage density per SWNT ranges from 5–10 mass%. Thus, the authors assumed the residual carbonaceous material (>99% of the sample) to be inert, contrary to the well-known fact that activated carbon is an excellent adsorber.[22,23] If the high-temperature peak were responsible for 5–10 mass% hydrogen, the low-temperature peak would deliver 25–100 mass% hydrogen. The authors also tried to measure the activation energy for the hydrogen desorption in the high-temperature peak around 300 K and found a value of 19.4 kJ mol^{-1}. Three years later in a report to the U.S. Department of Energy,[24] this peak had moved significantly upward, to 600 K. Apparently, the reported results[21] are inconsistent. Hirscher et al.[25] clarified the situation and showed that the desorption of hydrogen originates from Ti-alloy particles introduced during the ultrasonic treatment rather than from the CNTs.

The main differences between CNTs and high-surface-area graphite are the curvature of the graphene sheets and the cavity inside the tube. In microporous solids with capillaries that have a width not exceeding a few molecular diameters, the potential fields from opposite walls will overlap such that the attractive force acting on adsorbate molecules will be increased, as compared with that on a flat carbon surface.[26] This phenomenon is the main motivation for the investigation of hydrogen interaction with CNTs.

Most papers reporting theoretical studies on hydrogen absorption in carbon nanostructures focus on the physisorption of H_2 on carbon using the grand canonical Monte Carlo simulation. Stan and Cole[27] used the Feynman (semiclassical) effective potential approximation to calculate the adsorption potential and the amount of hydrogen adsorbed on a zigzag nanotube (13, 0) with a diameter of 1.018 nm. The adsorption potential was found to be 9 kJ mol^{-1} (0.093 eV) for hydrogen molecules inside the nanotubes at 50 K; the potential is about 25% higher than that of the flat surface of graphite, due to the curvature of the surface and, therefore, the increased number of carbon atoms interacting with the hydrogen molecule. The ratio of hydrogen adsorbed in the tube to that on a flat surface decreases strongly with increasing temperature and is 10,000 at 50 K and 100 at 77 K (values taken from Figure 2 in Reference 27). Rzepka et al.[28] used a grand canonical ensemble Monte Carlo program to calculate the amount of adsorbed hydrogen for a slit pore and a tubular geometry. The amount of adsorbed hydrogen depends on the surface area of the sample; the maximum is at 0.6 mass% (P = 6 MPa, T = 300 K). The calculation was verified experimentally with excellent agreement. At 77 K, the amount of adsorbed hydrogen is about one order of magnitude higher than that adsorbed at 300 K. Williams and Eklund[29] performed a grand canonical Monte Carlo simulation of H_2 physisorption in finite-diameter SWNT ropes and found an increasing amount of adsorbed hydrogen with decreasing temperature, from 1.4 mass% (P = 10 MPa, T = 300 K) to 9.6 mass% (P = 10 MPa, T = 77 K). For lower hydrogen pressure, this range is shifted to considerably lower amounts of adsorbed hydrogen: from 0.2 mass% (P = 1 MPa, T = 300 K) to 5.9 mass% (P = 1 MPa, T = 77 K). Lee et al.[30] have performed density functional and density functional-based tight-binding calculations to search for hydrogen chemisorption sites on SWNTs. The investigation of the absorption of the hydrogen inside the tubes has shown that it is energetically more favorable for the hydrogen atoms to recombine and form molecules, which are then physisorbed inside the nanotube. Ma et al.[31] performed a molecular-dynamics (MD) simulation for H implantation. The hydrogen atoms (20 eV) were implanted through the side walls of a SWNT (5, 5) consisting of 150 atoms and having a diameter of 0.683 nm. They found that the hydrogen atoms recombine to form molecules inside the tube and arrange themselves in a concentric tube. The hydrogen pressure inside the SWNT increases as the number of injected atoms increases and reaches 35 GPa for 90 atoms (5 mass%). This simulation does not exhibit a condensation of hydrogen inside the nanotube. The critical temperature of hydrogen (H_2) is 33.25 K.[32] Therefore, at temperatures above 33.25 K and at all pressures, hydrogen does not exist as a liquid phase; hydrogen is either a gas or a solid. The density of liquid and solid hydrogen at the melting point (T_m = 14.1 K) is 70.8 kg m^{-3} and 70.6 kg m^{-3}, respectively. Measurement of the latent heat of condensation of nitrogen on carbon black[33] showed that the heat for the adsorption of one monolayer is between 11 and 12 kJ mol^{-1} (0.11–0.12 eV) and decreases for subsequent layers to the latent heat of condensation for nitrogen, which is 5.56 kJ mol^{-1} (0.058 eV). If we assume that hydrogen behaves similarly to nitrogen, hydrogen would only form one monolayer of liquid at the surface of carbon at temperatures above the boiling point. Geometrical considerations of the nanotubes lead to the specific surface area and, therefore, to the maximum amount of condensed hydrogen in a surface monolayer. Figure 1 shows the maximum amount of hydrogen in mass% for the physisorption of hydrogen on CNTs.[34] The maximum amount of adsorbed hydrogen is 3.3 mass% and was found for SWNTs with a specific surface area of 1315 $m^2\ g^{-1}$.

Experiments on hydrogen absorption in carbon nanostructures were carried out with different methods under various conditions and on plenty of small and often not very well-characterized samples. Hydrogen-gas-adsorption isotherms (T = 80 K) on purified SWNT samples were performed by Ye et al.[35] The BET (Brunauer–Emmett–Teller) surface area of the SWNT sample was found to be 285 $m^2\ g^{-1}$ and remained unchanged upon hydrogen absorption and desorption. The hydrogen adsorption obtained at a temperature of 80 K and a pressure of 0.32 MPa was H/C (ratio of hydrogen to carbon atoms) = 0.04 for the SWNT sample and H/C = 0.28 for the high-surface-area saran-carbon (1600 $m^2\ g^{-1}$). Saran-carbon results from the pyrolysis of saran, a brand name for polyvinylidene chloride. At high hydrogen pressures (7 MPa) at a temperature of 80 K, the hydrogen-to-carbon ratio for the SWNT sample reached H/C = 1 (7.7 mass%) in the initial absorption. In the following absorption cycles, the absorption isotherm was considerably shifted to higher pressure, and a hydrogen-to-carbon ratio of H/C = 0.8 was reached at 12 MPa. Liu et al.[36] applied high-pressure (12 MPa) hydrogen gas at room temperature (298 K) to

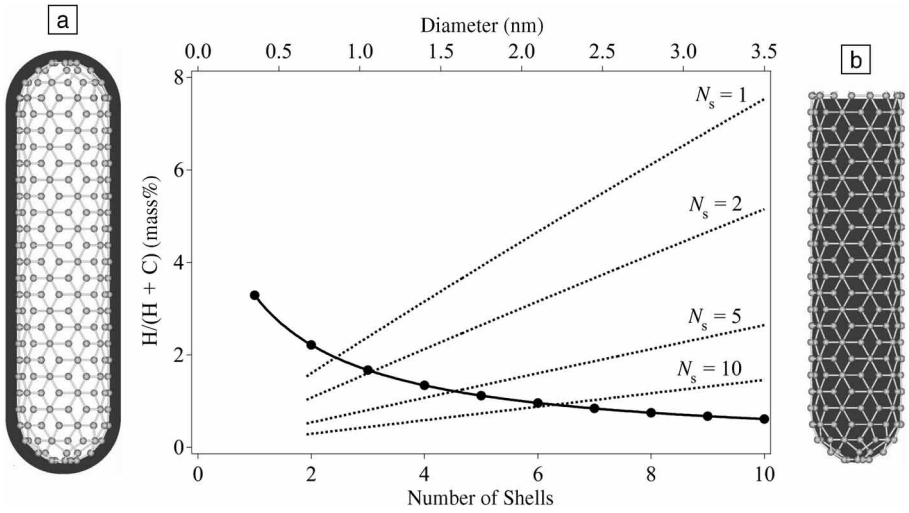

Figure 1. Calculated amount of adsorbed hydrogen in carbon nanotubes, assuming condensation of one monolayer of hydrogen. (a) Monolayer adsorbed at the outer surface (1315 $m^2\ g^{-1}$ for single-walled nanotubes) as a function of the number of shells (N_s) (bottom axis). (b) Cavity of the nanotube filled with liquid hydrogen as a function of the nanotube diameter (top axis).

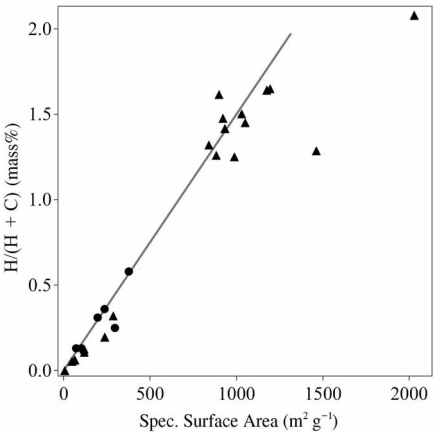

Figure 2. Reversible amount of hydrogen (electrochemical measurement at 298 K) versus the Brunauer–Emmett–Teller surface area (solid circles) of a few carbon nanotube samples, including two measurements on high-surface-area graphite samples, together with the fitted line. Hydrogen-gas-adsorption measurements at 77 K from Nijkamp et al.[41] (solid triangles) are included.

SWNTs and followed the pressure change in time. The samples equilibrated after approximately 300 min and reached a maximum absorption of 4.2 mass% (H/C = 0.5). About 20% of the absorbed hydrogen remained in the sample after desorption at room temperature. Fan et al.[37] investigated the hydrogen absorption of vapor-grown carbon nanofibers with diameters of 5–300 nm. The fibers absorbed up to 12.38 mass% hydrogen when a hydrogen pressure of 12 MPa was applied. The absorption equilibrated after 200–300 min. Chen et al.[38] reported that a high hydrogen uptake of 14 mass% can be achieved for K-doped MWNTs, and 20 mass% for Li-doped MWNTs, at a pressure of 0.1 MPa. The K-doped MWNTs absorb hydrogen at room temperature, but they are chemically unstable, whereas the Li-doped MWNTs are chemically stable, but require elevated temperatures (473–673 K) for maximum absorption and desorption of hydrogen. However, the increase of the mass observed upon hydrogen absorption was due to impurities such as oxygen and water and, therefore, the oxidation of the alkali metals[39] rather than a hydrogen uptake. A large variety of carbon samples were investigated using a high-pressure microbalance by Ströbel et al.[40] The BET (N_2) surface area of the samples ranged from 100 $m^2\ g^{-1}$ up to 3300 $m^2\ g^{-1}$. The absorbed amount of hydrogen (P = 12.5 MPa, T = 296 K) correlates with the specific surface area S according to the equation x(mass%) = 0.0005S($m^2\ g^{-1}$) (taken from Figure 3 in Reference 40), except for the nanofiber samples. The latter exhibit a rather low surface area of approximately 100 $m^2\ g^{-1}$; however, the increase in mass upon hydrogen absorption corresponds to about 1.2 mass%. The adsorption isotherms measured approximately follow the Langmuir adsorption model. Some isotherms intercept the mass axis (P = 0) at x = 0; others intercept at a finite mass between 0.2 mass% and 0.4 mass%, indicating an experimental error. Nijkamp et al.[41] characterized a large number of carbonaceous sorbents using N_2 physisorption at 77 K and a pressure of up to 1 bar. The sorbents were chosen to represent a large variation in surface areas and (micropore) volumes. Both nonporous materials such as aerosil and graphites and microporous sorbents such as activated carbons and zeolites were selected. The H_2 adsorption measurements were performed at 77 K in the pressure range of 0–1 bar. From adsorption–desorption experiments, it is evident that reversible physisorption exclusively takes place with all samples. The amount of adsorbed hydrogen correlates well with the specific surface area of the sample (Figure 2). A few papers on electrochemical measurements at room temperature of hydrogen uptake and release have been published.[42–45] The electrochemical hydrogen absorption is reversible. The maximum discharge capacity measured at 298 K is 2 mass% with a very small discharge current (discharge process for 1000 h). The few round markers together with the fitted line in Figure 2 are electrochemical results. It is remarkable that the measurements of the hydrogen uptake in the gas phase at 77 K exhibit the same quantities as the electrochemical measurements at room temperature (298 K). In the electrochemical charge process, hydrogen atoms are left at the surface of the electrode when the electron transfer from the conductor to the water molecules takes place. The hydrogen atoms recombine to form hydrogen molecules. This process goes on until the surface is completely covered with a monolayer of physisorbed H_2 molecules. Any further hydrogen does not interact with the attractive van der Waals forces of the surface. The hydrogen molecules become very mobile and form gas bubbles, which are released from the electrode surface. The formation of a stable monolayer of hydrogen at the electrode surface at room temperature is only possible if either the hydrogen atoms or the hydrogen molecules are immobile, that is, their surface diffusion has to be kinetically hindered by a large energy barrier, probably due to the adsorbed electrolyte (H_2O) molecules in the second layer. Another possible reaction path was first reported[30] as a result of density functional calculations and will be described in detail in the next section. The result of the calculation is that hydrogen atoms tend to chemisorb at the exterior surface of a nanotube. The atoms can then flip into the nanotube and, at high coverage, finally recombine into hydrogen molecules, forming a concentric

cylinder in the cavity of the nanotube. If the binding energy of the chemisorbed hydrogen is relatively low, as compared with the energy in hydrocarbons, the absorbed amount of hydrogen is proportional to the surface area of the carbon sample and could also desorb at a rather positive electrochemical potential.

In conclusion, the reversible hydrogen-sorption process is based on physisorption. The amount of adsorbed hydrogen is proportional to the BET surface area of the nanostructured carbon sample. The amount of hydrogen adsorbed from the gas phase at 77 K and electrochemically at room temperature is 1.5 mass% for a sample with a surface area of 1000 $m^2\ g^{-1}$. Together with the maximum specific surface area of carbon (1315 $m^2\ g^{-1}$), the maximum absorption capacity of carbon nanostructures is 2 mass%. No evidence was found for an influence of the geometric structure of the nanostructured carbon on the amount of hydrogen absorbed. Furthermore, all attempts to open the nanotubes and absorb hydrogen inside the tubes did not result in increased absorption of hydrogen molecules. Theoretical studies beyond the well-known physisorption led to a large set of various maximum hydrogen-absorption capacities. Most of the results were found under special conditions, for example, at 0 K or with high-energy hydrogen-atom implantation. No evidence was found for a higher density of hydrogen in and on carbon nanostructures, as compared with liquid hydrogen under ambient conditions.

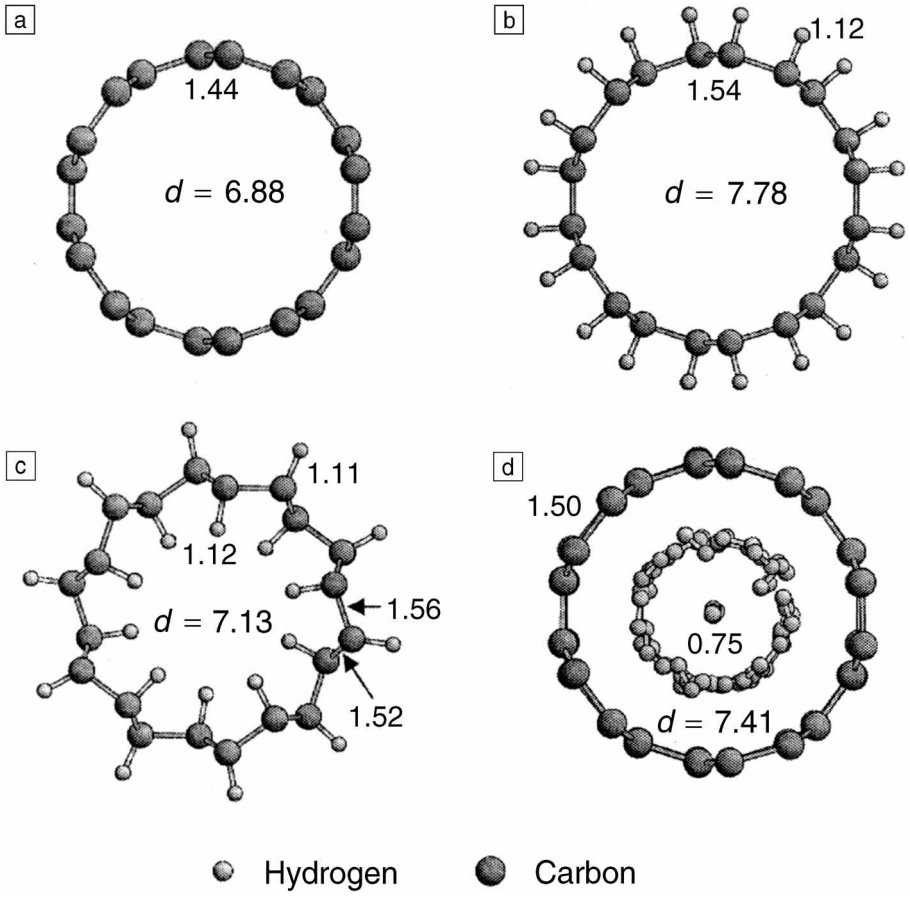

*Figure 3. Schematic illustrations of top views of various hydrogen adsorptions in a nanotube.[30] The numbers in the illustrations indicate the interatomic distances and the nanotube diameters (*d*) in angstroms. (a) Clean (5,5) nanotube; (b) arch type, where hydrogen atoms are chemisorbed at the exterior of the tube wall with a surface coverage $\Theta = 1.0$, $H/C = 1$ (7.7 mass%); (c) zigzag type, where hydrogen atoms are chemisorbed alternatively at the exterior and the interior of the tube wall with $\Theta = 1.0$, $H/C = 1$ (7.7 mass%); and (d) molecular hydrogen existing in an empty space in the nanotube with $\Theta \geq 1.0$, $H/C > 1$ (>7.7 mass%).*

Reaction with Atomic Hydrogen

Physisorbed hydrogen has a binding energy normally of the order of 0.1 eV, while chemisorbed hydrogen, normally regarded as having C–H covalent bonding, has a binding energy of more than 2–3 eV.

First, we summarize the calculations and simulations regarding hydrogen chemisorption on "ideal" carbon nanostructures. Lee and Lee have reported density functional and density functional-based tight-binding calculations for predicting the chemisorption sites and hydrogen concentration in (5,5) SWNTs at 0 K.[30] Their calculations indicated that there are two energetically favored C–H coordination sites with H/C = 1 (7.7 mass%); the arch-type (Figure 3b) with chemisorbed hydrogen outside the nanotube (2.65 eV), and the zigzag-type (Figure 3c) with chemisorbed hydrogen alternatively outside and inside the nanotube (3.12 eV). The carbon atoms are radially reconstructed in the latter case, and this reconstruction might lead to the sp^3-like C–H coordination with a higher C–H binding energy. Reconstruction-assisted hydrogen chemisorption has also been reported by Jeloaica and Sidis[46] for the surface of graphite, at which hydrogen atoms are exclusively trapped on top of carbon atoms (Figures 4a and 4b). High-density chemisorbed hydrogen, on the other hand, is not stable inside the nanotube, and thus, hydrogen atoms were predicted to recombine into molecules. They estimated that more than 14 mass% of hydrogen (molecules) could be stored inside (10,10) nanotubes. The first-principles MD simulation reported by Tada et al.[47] also indicated that chemisorbed hydrogen is stable outside nanotubes, but not stable inside them. The C–H binding energy increases with decreasing tube diameter, due to the partial formation of sp^3-like components. Ma et al.[31] have also calculated the hydrogen-storage properties in (5,5) SWNTs using the model of hydrogen implantation with a kinetic energy of 16–25 eV. The implanted hydrogen atoms recombined into molecules inside the nanotubes, and hydrogen concentration reached 5 mass%. With MWNTs, Lee et al.[30] claimed that chemisorbed hydrogen is favored between the tube walls, and the predicted hydrogen concentration is 7–8 mass%, independent of tube diameter.

There are some experimental reports on chemisorbed hydrogen in carbon-related materials. The chemisorption processes in some graphite intercalation compounds (GICs) have been systematically studied by Enoki et al.[48] The alkali-metal GICs, such as C_8K, with Stage 1 structures (containing metallic elements in every interlayer of graphene) react with hydrogen above room temperature, and then dissociated hydrogen atoms enter the interlayer space

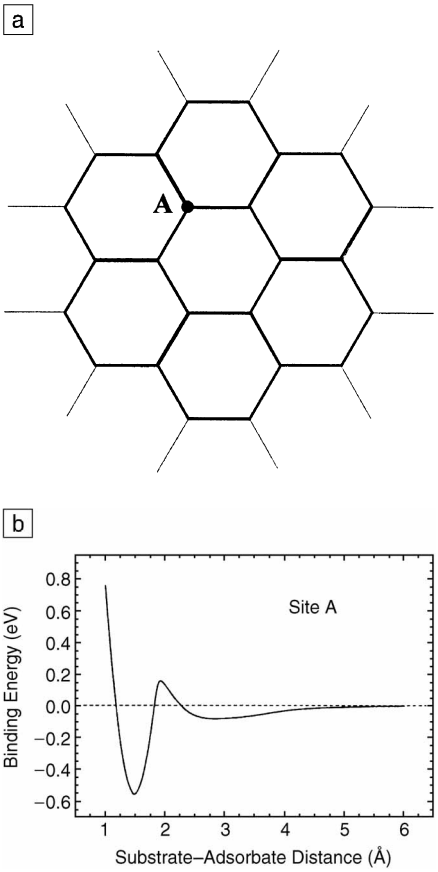

Figure 4. (a) Schematic model of a (0001) graphite surface used in the simulation by Jeloaica and Sidis,[46] and (b) calculated binding energy of a hydrogen atom on top of a "relaxed" carbon atom, site A.

between the alkali metals to form K^+-H^--K^+, that is, triple-atomic-layer sandwiches (Figure 5). The inserted two-dimensional hydrogen layer is suggested to consist of H^- ions with a weakly metallic nature. Maximum hydrogen concentration was $C_8KH_{0.67}$ (0.5 mass%) at ambient pressure, and the hydrogen-storage properties were reported to be reversible. The properties of the other GICs are described in detail by Enoki et al.[48] The chemisorption processes are also reported in fullerenes: C_{60} fullerenes were theoretically predicted to have a reversible hydrogen-storage reaction of up to $C_{60}H_{60}$ (7.7 mass%). Brosha et al.[49] have synthesized $C_{60}H_{18.7}$ (2.5 mass%) by means of direct reaction of fullerenes with hydrogen gas. This hydride was found to be stable up to 700 K, and the desorbed gas component at higher temperatures was a mixture of H_2 and CH_4. They reported that the hydrogen-storage properties were not reversible, due to the

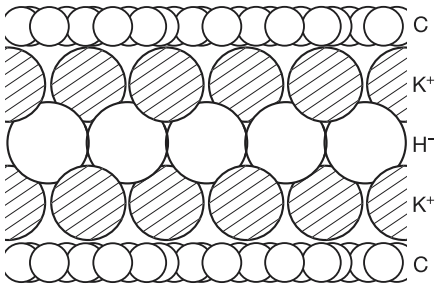

Figure 5. C_8K with K^+-H^--K^+ triple-atomic-layer sandwiches. (After Reference 48.)

transformation from the fullerenes into the planar graphite-like species at elevated temperatures. Loutfy and Wexler[50] have also reported on $C_{60}H_{46.8}$ (6.1 mass%) by hydrogenation at about 720 K under a hydrogen pressure of 3 MPa. Further experimental activities are planned to achieve reversible hydrogen-storage reactions.

The hydrogen-desorption properties of the pretreated nanotubes reported by Dillon et al.[21] strongly indicate that there is nonphysisorbed hydrogen desorbing around 600 K (although Hirscher et al.[25] have reported the desorption peak as mainly coming from the contaminated Ti alloys during sonication). Dillon et al.[21] have reported that hydrogen around 600 K was an intermediate state between physisorption and chemisorption. As already mentioned, the number of defects (e.g., dangling carbon bonds) in the nanotubes increases with pretreatments, and it is reasonable to assume that the defects provide trapping sites for weakly chemisorbed (bonded) hydrogen.

The maximum hydrogen concentration in highly defective graphite prepared by mechanical milling has been estimated at 7.4 mass%,[18] with two desorption peaks, starting around 600 K and 950 K, respectively.[20] At temperatures around the first desorption peak, small traces of the desorption peaks of hydrocarbons with mass numbers of 16 from CH_4 and of 28 from a fragment of C_2H_6 were also detected (Figure 6). The first desorption peak has a similar origin as the main desorption peaks around 600 K of SWNTs. Here, the apparent desorption temperatures tend to be modified by "kinetic" effects, depending on the amounts of metallic impurities, heating rates, and so on. No hydrocarbon has been found at temperatures where the second desorption peak appears (Pekker et al.[51] have reported two-step hydrogen desorption from nanotubes hydrogenated in liquid ammonia). Cracknell[52]

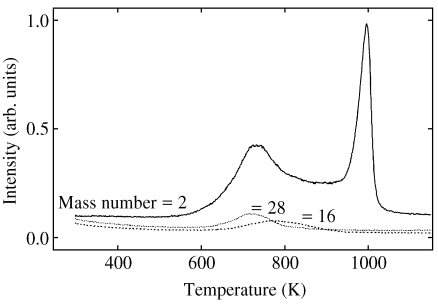

Figure 6. Thermal desorption mass spectroscopy of nanostructured graphite mechanically milled for 80 h under hydrogen atmosphere.[20] The combined analysis of the thermal desorption mass spectroscopy and thermogravimetry indicated that approximately 6 mass% of hydrogen (corresponding to 80% of the total hydrogen concentration) is desorbed at the first desorption peak as a mixture of pure hydrogen and hydrocarbons.

has assumed a weak chemical potential for hydrogen and calculated the hydrogen-storage properties by using the potential. The hydrogen concentration was estimated to reach 6 mass% under a hydrogen pressure of 1 MPa[52] (Figure 7). This estimated hydrogen concentration corresponds well to the experimental results mentioned earlier (Figure 6).

In conclusion, the existence of hydrogen in an intermediate state between physisorption and chemisorption (i.e., weakly bonded states) is scientifically unclear but surely of importance for the hydrogen-storage properties of carbon nanostructures. Also, defect structures induced by pre-

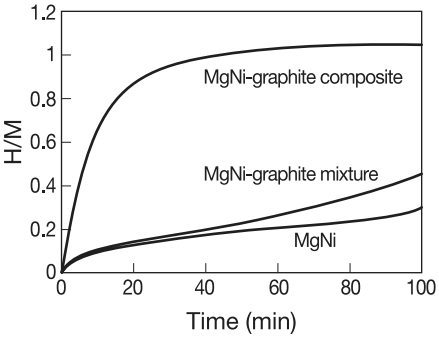

Figure 7. Hydrogen-storage kinetics of amorphous MgNi with and without surface modification by means of mechanical milling with graphite (MgNi-graphite composite) at room temperature.[73] The initial hydrogen pressure was 3 MPa.

treatment may provide trapping sites for hydrogen in an intermediate state.

Metallic Hydrogen

As was mentioned in the previous section, the inserted hydrogen layer in K-GICs ($C_{4n}KH_x$) is suggested to consist of densely packed two-dimensional sheets of H^- ions with a weakly metallic character.[48,53] If actually metallic, the system would be rather attractive not only from the hydrogen-storage viewpoint, but also from the superconductivity viewpoint, with a critical temperature (T_c) presumably in the range of 140–260 K.[54–57] So far, the superconductivity of hydrogenated K-GICs ($x \approx 0.8$) has not been proven, at least not under ambient pressure, but GICs with some hydrogen-rich layers may provide interesting metallic-hydrogen properties.[48] Besides the GICs, some complex metal hydrides, or so-called chemical hydrides, have been investigated for their possible metallic-hydrogen properties and high-T_c superconductivities. One of the controversial candidates is the Li-Be-H system or its B-substituted system, or Li-Be-H under high pressures.[58–62] The ultimate high-performance hydrogen-storage property will also provide the ultimate high-T_c superconductivity.

Hydrogen in Mg-Based Metallic Microstructures and Metal-Carbon Composites

Nanostructured Mg-Related Materials

Metallic nanostructured materials are reported to have specific properties in regard to their reactivity with hydrogen, in comparison with conventional (poly-) crystalline or amorphous metallic materials, in both thermodynamic and diffusional aspects.[63–65] Their properties are of great importance for hydrogen-storage functions, especially in Mg-related materials, which have high hydrogen capacities but low reactivities with hydrogen. For example, Zaluska et al.[66,67] have reported that polycrystalline Mg did not exhibit any significant hydrogen-storage reaction at 573 K, whereas the nanostructured Mg absorbed hydrogen readily, even during the first exposure and without any prior activation. Also, Liang et al. and Huot et al.[68–70] have pointed out that polycrystalline Mg does not desorb at 573 K, while the nanostructured Mg (after mechanical milling), especially with other metallic elements as catalysts, exhibits a much faster desorption reaction. Orimo and Fujii[71] have recently summarized the close relationship between nanometer- or atom-scale structures and the specific hydrogen-storage properties of the Mg-Ni binary system.

Graphite-Mg Composites

Graphite is found to have some advantages for the surface modification of Mg-related materials. Iwakura et al.[72] and Nohara et al.[73] have reported that surface modification of Mg-related materials by mechanical milling with graphite effectively improved the physicochemical and electrochemical properties of the samples.[73–75] For example, the hydrogen-storage kinetics of amorphous MgNi at room temperature increased after the surface modification, mainly due to an increase in the Ni/Mg ratio on the alloy surface (Figure 7). C-Mg composite systems prepared by mechanical milling both of graphite and Mg with organic additives (cyclohexane, benzene, or tetrahydrofuran) have been proposed by Imamura et al.[76-79] The binding energy of Mg 2*p* in the samples prepared with organic additives is shifted by 0.32–0.85 eV to higher energies, while there is no shift for the composites obtained without additives. Such charge-transfer sites are known to be usually active for the catalytic activation of hydrogen molecules. The composites prepared without any additives show only a very low activity for hydrogen. Imamura et al. have also pointed out that the formation of nanometer-scale composites, that is, nanocomposites, leads not only to the increase in hydrogen-storage kinetics, but also to the appearance of additional hydrogen trapping sites (in addition to within Mg itself). These new hydrogen trapping sites seem to relate to the defective structures in carbon-related materials, as mentioned earlier.

Acknowledgment

Financial support from the Swiss Federal Office of Energy (BfE, Bundesamt für Energiewirtschaft) and the Swiss Federal Office for Science and Education (BBW, Bundesamt für Bildung und Wissenschaft) FUCHSIA EU5 project is acknowledged.

References

1. S. Iijima, *Nature* **354** (1991) p. 56.
2. N. Hamada, S. Sawada, and A. Oshiyama, *Phys. Rev. Lett.* **68** (1992) p. 54.
3. M.S. Dresselhaus, G. Dresselhaus, and P. Eklund, *Science of Fullerenes and Carbon Nanotubes* (Academic Press, New York, 1996).
4. F. Darkrim and D. Levesque, *J. Chem. Phys.* **109** (1998) p. 4981.
5. R.G. Ding, G.Q. Lu, Z.F. Yan, and M.A. Wilson, *J. Nanosci. Nanotechnol.* **1** (2001) p. 7.
6. M. Monthioux, B.W. Smith, B. Burteaux, A. Claye, J.E. Fischer, and D.E. Luzzi, *Carbon* **39** (2001) p. 1251.
7. M. Nakamizo, H. Honda, and M. Inagaki, *Carbon* **16** (1978) p. 281; L. Nikiel and P.W. Jagodzinski, *Carbon* **31** (1993) p. 1313.
8. K. Niwase, T. Tanaka, Y. Kakimoto, K.N. Ishihara, and P.H. Shingu, *Mater. Trans., JIM* **36** (1995) p. 282.
9. T.D. Shen, W.Q. Ge, K.Y. Wang, M.X. Quan, J.T. Wang, W.D. Wei, and C.C. Koch, *Nanostruct. Mater.* **7** (1996) p. 393.
10. J. Tang, W. Zhao, L. Li, A.U. Falster, W.B. Simmons Jr., W.L. Zhou, Y. Ikuhara, and J.H. Zhang, *J. Mater. Res.* **11** (1996) p. 733.
11. T. Fukunaga, K. Nagano, U. Mizutani, H. Wakayama, and Y. Fukushima, *J. Non-Cryst. Solids* **232–234** (1998) p. 416.
12. F. Salver-Disma, J.M. Tarascon, C. Clinard, and J.N. Rouzaud, *Carbon* **37** (1999) p. 1941.
13. J.Y. Huang, *Acta Mater.* **47** (1999) p. 1801.
14. J.Y. Huang, H. Yasuda, and H. Mori, *Chem. Phys. Lett.* **303** (1999) p. 130.
15. Y. Chen, J.F. Gerald, L.T. Chadderton, and L. Chaffron, *Appl. Phys. Lett.* **74** (1999) p. 2782.
16. T.S. Ong and H. Yang, *Carbon* **38** (2000) p. 2077.
17. X.H. Chen, H.S. Yang, G.T. Wu, M. Wang, F.M. Deng, X.B. Zhang, J.C. Peng, and W.Z. Li, *J. Cryst. Growth* **218** (2000) p. 57.
18. S. Orimo, G. Majer, T. Fukunaga, A. Züttel, L. Schlapbach, and H. Fujii, *Appl. Phys. Lett.* **75** (1999) p. 3093.
19. T. Fukunaga, K. Itoh, S. Orimo, M. Aoki, and H. Fujii, *J. Alloys Compd.* **327** (2001) p. 224.
20. S. Orimo, T. Matsushima, H. Fujii, T. Fukunaga, and G. Majer, *J. Appl. Phys.* **90** (2001) p. 1545.
21. A.C. Dillon, K.M. Jones, T.A. Bekkedahl, C.H. Kiang, D.S. Bethune, and M.J. Heben, *Nature* **386** (1997) p. 377.
22. S. Hynek, W. Fuller, and J. Bentley, *Int. J. Hydrogen Energy* **22** (6) (1997) p. 601.
23. P. Bénard and R. Chahine, *Int. J. Hydrogen Energy* **26** (2001) p. 849.
24. A.C. Dillon, T. Gennett, J.L. Alleman, K.M. Jones, P.A. Parilla, and M.J. Heben, in *Proc. 2000 U.S. DOE/NREL Hydrogen Program Review,* Vol. II, NREL/CP-570-28890 (National Renewable Energy Laboratory, Golden, CO, 2000).
25. M. Hirscher, M. Becher, M. Haluska, U. Dettlaff-Weglikowska, A. Quintel, G.S. Duesberg, Y.M. Choi, P. Downes, M. Hulman, S. Roth, I. Stepanek, and P. Bernier, *Appl. Phys. A* **72** (2001) p. 129.
26. S.J. Gregg and K.S.W. Sing, *Adsorption, Surface Area and Porosity* (Academic Press, London, 1967).
27. G. Stan and M.W. Cole, *J. Low Temp. Phys.* **110** (1998) p. 539.
28. M. Rzepka, P. Lamp, and M.A. de la Casa-Lillo, *J. Phys. Chem. B* **102** (1998) p. 10849.
29. K.A. Williams and P.C. Eklund, *Chem. Phys. Lett.* **320** (2000) p. 352.
30. S.M. Lee, K.H. An, Y.H. Lee, G. Seifert, and T. Frauenheim, *J. Korean Phys. Soc.* **38** (2001) p. 686; S.M. Lee and Y.H. Lee, *Appl. Phys. Lett.* **76** (2000) p. 2879.
31. Y. Ma, Y. Xia, M. Zhao, R. Wang, and L. Mei, *Phys. Rev. B* **63** 115422 (2001).
32. W.B. Leung, N.H. March, and H. Motz, *Phys. Lett.* **56** (1976) p. 425.
33. R.A. Beebe, J. Biscoe, W.R. Smith, and C.B. Wendell, *J. Am. Chem. Soc.* **69** (1947) p. 95.

34. A. Züttel, P. Sudan, Ph. Mauron, T. Kiyobayashi, Ch. Emmenegger, and L. Schlapbach, *Int. J. Hydrogen Energy* **27** (2002) p. 203.
35. Y. Ye, C.C. Ahn, C. Witham, B. Fultz, J. Liu, A.G. Rinzler, D. Colbert, K.A. Smith, and R.E. Smalley, *Appl. Phys. Lett.* **74** (1999) p. 2307.
36. C. Liu, Y.Y. Fan, M. Liu, H.T. Cong, H.M. Cheng, and M.S. Dresselhaus, *Science* **286** (1999) p. 1127.
37. Y.Y. Fan, B. Liao, M. Liu, Y.L. Wei, M.Q. Lu, and H.M. Cheng, *Carbon* **37** (1999) p. 1649.
38. P. Chen, X. Wu, J. Lin, and K.L. Tan, *Science* **285** (1999) p. 91.
39. M. Hirscher, M. Becher, M. Haluska, A. Quintel, V. Skakalova, Y.M. Choi, U. Dettlaff-Weglikowska, S. Roth, I. Stepanek, P. Bernier, A. Leonhardt, and J. Fink, *J. Alloys Compd.* **330–332** (2002) p. 654.
40. R. Ströbel, L. Jörissen, T. Schliermann, V. Trapp, W. Schütz, K. Bohmhammel, G. Wolf, and J. Garche, *J. Power Sources* **84** (1999) p. 221.
41. M.G. Nijkamp, J.E.M.J. Raaymakers, A.J. van Dillen, and K.P. de Jong, *Appl. Phys. A* **72** (2001) p. 619.
42. Ch. Nützenadel, A. Züttel, and L. Schlapbach, in *Science and Technology of Molecular Nanostructures,* Chapter 9, edited by H. Kuzmany, J. Fink, M. Mehring, and S. Roth (American Institute of Physics, New York, 1999) p. 462.
43. Ch. Nützenadel, A. Züttel, Ch. Emmenegger, P. Sudan, and L. Schlapbach, in *Science and Applications of Nanotubes,* Chapter 10, Fundamental Materials Research Series, edited by M.F. Thorpe (Kluwer Academic/Plenum Publishers, New York, 2000) p. 205.
44. A. Züttel, P. Sudan, Ph. Mauron, Ch. Emmenegger, T. Kiyobayashi, and L. Schlapbach, *J. Metastable Nanocryst. Mater.* **11** (2001) p. 95.
45. S.M. Lee, K.S. Park, Y.C. Choi, Y.S. Park, J.M. Bok, D.J. Bae, K.S. Nahm, Y.G. Choi, S.Ch. Yu, N. Kim, T. Frauenheim, and Y.H. Lee, *Synth. Met.* **113** (2000) p. 209.
46. L. Jeloaica and V. Sidis, *Chem. Phys. Lett.* **300** (1999) p. 157.
47. K. Tada, S. Furuya, and K. Watanabe, *Phys. Rev. B* **63** 155405 (2001).
48. T. Enoki, S. Miyajima, M. Sano, and H. Inokuchi, *J. Mater. Res.* **5** (1990) p. 435.
49. E.L. Brosha, J. Davey, F.H. Garzon, and S. Gottesfeld, *J. Mater. Res.* **14** (1999) p. 2138.
50. R.O. Loutfy and E.M. Wexler, in *Proc. 2001 DOE Hydrogen Program Review,* NREL/CP-570-30535 (National Renewable Energy Laboratory, Golden, CO, 2001).
51. S. Pekker, J.-P. Salvetat, E. Jakab, J.-M. Bonard, and L. Forro, *J. Phys. Chem. B* **105** (2001) p. 7938.
52. R.F. Cracknell, *Phys. Chem. Chem. Phys.* **3** (2001) p. 2091.
53. S. Miyajima, M. Kabasawa, T. Chiba, T. Enoki, Y. Maruyama, and H. Inokuchi, *Phys. Rev. Lett.* **64** (1990) p. 319.
54. N.W. Ashcroft, *Phys. Rev. Lett.* **21** (1968) p. 1748.
55. T. Schneider, *Helv. Phys. Acta* **42** (1969) p. 957.
56. L.G. Caron, *Phys. Rev. B* **9** (1974) p. 5025.
57. D.A. Papaconstantopoulos, L.L. Boyer, B.M. Klein, A.R. Williams, V.L. Morruzzi, and J.F. Janak, *Phys. Rev. B* **15** (1977) p. 4221.
58. A.W. Overhauser, *Phys. Rev. B* **35** (1987) p. 411.
59. M.R. Press, B.K. Rao, and P. Jena, *Phys. Rev. B* **38** (1988) p. 2380.
60. R. Yu and P.K. Lam, *Phys. Rev. B* **38** (1988) p. 3576.
61. J.L. Martins, *Phys. Rev. B* **38** (1988) p. 12776.
62. M. Seel, A.B. Kunz, and S. Hill, *Phys. Rev. B* **39** (1989) p. 7949.
63. T. Mütschele and R. Kirchheim, *Scripta Metall.* **21** (1987) p. 135.
64. T. Mütschele and R. Kirchheim, *Scripta Metall.* **21** (1987) p. 1101.
65. R. Kirchheim, T. Mütschele, W. Kieninger, H. Gleiter, R. Birringer, and T.D. Koblé, *Mater. Sci. Eng.* **99** (1988) p. 457.
66. A. Zaluska, L. Zaluski, and J.O. Ström-Olsen, *J. Alloys Compd.* **288** (1999) p. 217.
67. A. Zaluska, L. Zaluski, and J.O. Ström-Olsen, *Appl. Phys. A* **72** (2001) p. 157.
68. G. Liang, J. Huot, S. Boily, A.V. Neste, and R. Schulz, *J. Alloys Compd.* **291** (1999) p. 295.
69. G. Liang, J. Huot, S. Boily, and R. Schulz, *J. Alloys Compd.* **305** (2000) p. 239.
70. J. Huot, G. Liang, and R. Schulz, *Appl. Phys. A* **72** (2001) p. 187.
71. S. Orimo and H. Fujii, *Appl. Phys. A* **72** (2001) p. 167.
72. C. Iwakura, S. Nohara, H. Inoue, and Y. Fukumoto, *Chem. Commun.* (15) (1996) p. 1831.
73. S. Nohara, H. Inoue, Y. Fukumoto, and C. Iwakura, *J. Alloys Compd.* **252** (1997) p. L16.
74. C. Iwakura, H. Inoue, S.G. Zhang, S. Nohara, K. Yorimitsu, N. Kuramoto, and T. Morikawa, *J. Electrochem. Soc.* **146** (1999) p. 1659.
75. C. Iwakura, H. Inoue, S.G. Zhang, and S. Nohara, *J. Alloys Compd.* **293–295** (1999) p. 653.
76. H. Imamura, N. Sakasai, and Y. Kajii, *J. Alloys Compd.* **232** (1996) p. 218.
77. H. Imamura, N. Sakasai, and T. Fujinaga, *J. Alloys Compd.* **253–254** (1997) p. 34.
78. H. Imamura, Y. Takesue, T. Akimoto, and S. Tabata, *J. Alloys Compd.* **293–295** (1999) p. 564.
79. H. Imamura, S. Tabata, Y. Takesue, Y. Sakata, and S. Kamazaki, *Int. J. Hydrogen Energy* **25** (2000) p. 837. □